

Anomalous Temperature Dependence of Quantum Correction to the Conductivity of Magnetic Topological Insulators

Huan-Wen Wang, Bo Fu, and Shun-Qing Shen*

Department of Physics, The University of Hong Kong, Pokfulam Road, Hong Kong, China

Quantum transport in magnetic topological insulators reveals strong interplay between magnetism and topology of electronic band structures. A recent experiment on magnetically doped topological insulator Bi_2Se_3 thin films showed the anomalous temperature dependence of the magnetoconductivity while their field dependence presents a clear signature of weak anti-localization [Tkac *et al.*, PRL 123, 036406(2019)]. Here we demonstrate that the tiny mass of the surface electrons induced by the bulk magnetization leads to a temperature-dependent correction to the π Berry phase, and generates a decoherence mechanism to the phase coherence length of the surface electrons. As a consequence, the quantum correction to conductivity can exhibit non-monotonic behavior by decreasing temperature. This effect is attributed to the close relation of the Berry phase and quantum interference of the topological surface electrons in quantum topological materials.

Introduction. Three-dimensional (3D) topological insulators (TIs) have stimulated intensive theoretical and experimental study in the past decade [1–6]. In the quantum diffusive regime, owing to the nontrivial π Berry's phase, the topological surface states are expected to experience a destructive quantum interference in the scattering process [7–10]. Accordingly, the magnetoconductivity shows a negative notch in a weak magnetic field (B) and is called weak anti-localization (WAL), which has been regarded as significant transport signature for the topological surface states of TIs [11–16]. Besides, one anticipates that the conductivity correction from the WAL effect should decrease with increasing the temperature. However, the temperature dependence of conductivity usually shows an opposite tendency in experiments [17–22]. Such a dilemma in some pristine TIs can be resolved by further considering the electron-electron interaction effect at low temperatures [23–25]. Recently, Tkac *et al.* reported that the contradictory tendency between the temperature- and magnetic-field-dependent conductivity remains even after subtracting the interaction effect in the Mn-doped Bi_2Se_3 thin films [26]. As shown in Fig. 1, the magnetoconductivity $\delta\sigma(B)$ exhibits monotonic temperature dependence for a non-doped Bi_2Se_3 sample, a typical behavior of WAL as expected theoretically, and a non-monotonic temperature dependence for the doped ($x_{\text{Mn}} = 4\%$ and $x_{\text{Mn}} = 8\%$) samples, respectively, where $\delta\sigma(B) = \sigma(T, B) - \sigma(T, 0)$ with $\sigma(T, B)$ the temperature-dependent conductivity at a finite magnetic field B . At low temperatures, the doped and non-doped samples show opposite temperature dependence. Meanwhile, the magnetoconductivity for those samples always exhibit WAL correction as shown in Fig. 2 in [26]. The simple assumption of the monotonic temperature dependence of coherence length due to the electron-electron interaction effect [23, 24, 27] cannot account for these observations. Actually, the surface state in the magnet-

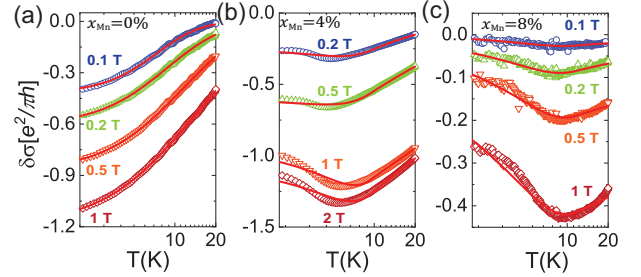


Figure 1. Magnetoconductivity as a function of temperature at different magnetic field strength for two Mn-doped Bi_2Se_3 thin films of Mn-doped concentration (a) $x_{\text{Mn}} = 0\%$, (b) $x_{\text{Mn}} = 4\%$, and (c) $x_{\text{Mn}} = 8\%$. The open squares are the experimental data extract from Ref. [26]. The solid red lines are the fitting results at different magnetic field B by using the formula in Eq. (6).

ically doped TIs acquires a finite mass due to the time-reversal symmetry breaking accompanied with a small correction to the π Berry phase [28–32]. The nearly π Berry phase is capable of accounting for the WAL behavior for the magnetoconductivity but fails to explain the anomalous behavior.

In this Letter, we resolve the puzzle of the anomalous temperature dependence of quantum correction. The role of the magnetic doping is assumed to produce a finite gap for the surface states. Then, a magnetoconductivity formula of quantum interference is derived for massive Dirac fermions, which is simply characterized by the spin polarization η . The quantity is also associated to the correction to the π Berry phase of surface electrons. The nearly π Berry phase accounts for the WAL behavior for the magnetoconductivity. However, the temperature dependence of η leads to a non-monotonic behavior of the quantum correction to the conductivity at low temperatures due to the quantum decoherence effect caused by the deviation from the π Berry phase. The good coincidence between our theory and experimental data suggests that the anomalous temperature dependence can

* sshen@hku.hk

be ascribed to the temperature-dependent correction to the π Berry phase of the surface states.

Model Hamiltonian and spin polarization. Due to the hybridization of the top and bottom surface states or the time-reversal symmetry breaking caused by the magnetic doping, the surface electrons in the TI thin films can acquire a finite mass [28, 33–35], thus it is proper to treat the surface states as massive Dirac fermions. Besides, in a TI thin film, the 3D bulk band is quantized into two-dimensional (2D) sub-bands owing to the quantum confinement effect. The 2D sub-bands have a similar low energy Hamiltonian as the surface one but with a relatively large band gap [36]. We begin with the modified model of 2D massive Dirac fermions [5, 34],

$$H = v\hbar(\sigma_x k_x + \sigma_y k_y) + m(k)\sigma_z \quad (1)$$

where v is the effective velocity, \hbar is the reduced Planck constant, $\sigma_{x,y,z}$ are the Pauli matrices, $\mathbf{k} = (k_x, k_y)$ is the wave vector, and $m(k) = mv^2 - b\hbar^2(k_x^2 + k_y^2)$ is the mass term, and m and b are the coefficients. The mass term gives the spin polarization $\eta = \langle \sigma_z \rangle = m(k_F)/\sqrt{v^2\hbar^2k_F^2 + [m(k_F)]^2}$ at the Fermi radii k_F , which is directly related to the Berry phase for Dirac fermions. As shown in Fig. 2, the spin lies in the plane of the Fermi circle for $\eta = 0$ and is tilted to the out of plane for $\eta \neq 0$. After the spin vector travels along the Fermi circle adiabatically, a Berry phase is acquired, $\phi_b = \frac{1}{2} \int_0^\pi \int_0^{\arccos \eta} \sin \theta d\theta d\phi = \pi(1-\eta)$. Furthermore, we mark the spin and momentum orientation in the trajectory of backscattering and corresponding time-reversal trajectory. For $\eta = 0$, the spins of incoming (\mathbf{k}) and outgoing ($-\mathbf{k}$) electrons are anti-parallel to each other. The scattering sequences are accompanied by the coherent spin rotation which yields the WAL due to the π Berry phase. For $\eta \neq 0$, the spin of the $(\mathbf{k}, -\mathbf{k})$ electron pair is partially tilted to the z -direction, and the spin-singlet and triplet pairings mix together. Consequently, the accumulating Berry phase deviates from π , and after taking the average of all the possible trajectories with different winding numbers, a new decoherence mechanism is introduced. When $\eta \rightarrow 1$, the spin is along the z -direction. The incoming and outgoing electrons form a triplet pairing and give rise to a WL correction.

Cooperon gaps and weighting factors. The quantum correction to the conductivity is evaluated by using the Feynman diagrammatic technique [37–42]. In the present calculation, we keep the matrix form for Green's functions and treat all possible Cooperon channels, correlators in the particle-particle pairing channels in electric conductivity of non-superconducting metals, on the same footing [43]. In the diffusion approximation, it is found that three out of four possible Cooperon channels contribute to the conductivity,

$$\sigma_{\text{qi}} = -\frac{4e^2}{h} \sum_i \sum_q \frac{w_i}{\ell_i^{-2} + q^2} \quad (2)$$

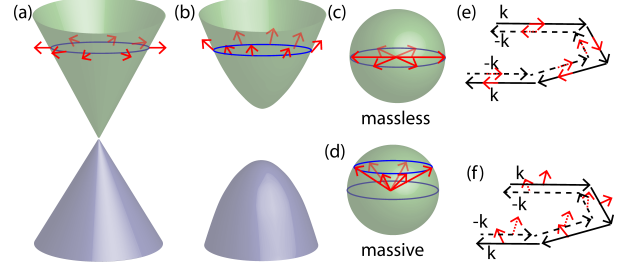


Figure 2. Schematic diagram of the band structure and spin orientation for (a) massless and (b) massive Dirac fermions. The spin vectors at a certain Fermi energy are depicted by the red arrows. (c) and (d) show the corresponding Berry phase as the solid angle traced out the spin vectors on the Bloch sphere for (a) and (b), respectively. (e) and (f) show the trajectory of backscattering (solid line) and corresponding time-reversal trajectory (dashed line) for massless and massive Dirac fermions, respectively. The black arrow represents the momentum direction, and the red arrow denotes the spin orientation.

Table I. The components of four Cooperon channels $i = s, t_0, \pm$ in the basis of spin-triplet and singlet $|s, s_z\rangle$, the Cooperon gap ℓ_i^{-2} in unit of the mean free path ℓ_e^{-2} and the weighting factors w_i .

i	Cooperon in $ s, s_z\rangle$	w_i	ℓ_i^{-2}/ℓ_e^{-2}
s	$ 0, 0\rangle$	$-\frac{(1-\eta^2)^2}{2(1+3\eta^2)^2}$	$\frac{(1-\eta^2)\eta^2}{(1+\eta^2)^2}$
t_+	$ 1, 1\rangle$	$\frac{4\eta^2(1+\eta^2)}{(1+3\eta^2)^2}$	$\frac{4(1-\eta)^2\eta^2}{(1+3\eta^2)(1+\eta)^2}$
t_0	$ 1, 0\rangle$	0	∞
t_-	$ 1, -1\rangle$	$\frac{4\eta^2(1+\eta^2)}{(1+3\eta^2)^2}$	$\frac{4(1+\eta)^2\eta^2}{(1+3\eta^2)(1-\eta)^2}$

where $i = s, t_+, t_-$ is the Cooperon channel index, ℓ_i^{-2} and w_i are the corresponding Cooperon gap and weighting factors, respectively. The expressions for ℓ_i^{-2} and w_i are listed in Table I.

The channels $i = t_{\pm}$ contribute to the WL correction, and the channel s contributes to the WAL correction according to the signs of their weighting factors $w_{t_{\pm}} > 0$ and $w_s < 0$. The original Cooperon structure factor $\Gamma(q)$ is in the basis of $\{|\uparrow\uparrow\rangle, |\uparrow\downarrow\rangle, |\downarrow\uparrow\rangle, |\downarrow\downarrow\rangle\}$. To diagonalize $\Gamma(q)$, we rotated the basis into the spin-singlet and triplet basis $|s, s_z\rangle$, where $|s, s_z\rangle$ labels the total spin $s (= 0, 1)$ and its z -component s_z . The channels $i = t_{\pm}$ correspond to the two triplet pairing ($s = 1$) and result in the WL correction, while the channel $i = s$ is the singlet pairing ($s = 0$) and gives out the WAL correction. ℓ_i^{-2} and w_i are plotted in Fig. 3. When $\eta = 0$ and $\phi_b = \pi$, one finds a pure WAL correction from the channel s , which is consistent with the Hikami-Larkin-Nagaoka formula for the strong spin-orbit scattering [38]. When $\eta = 1$

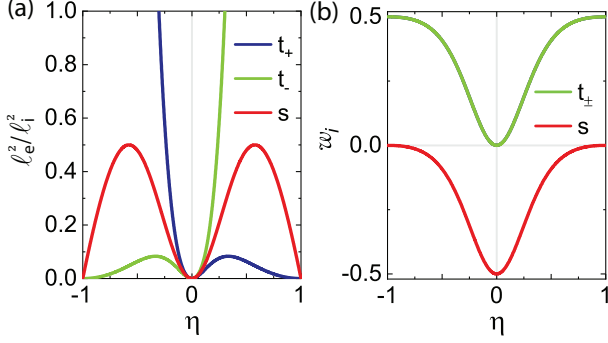


Figure 3. (a) The Cooperon gap ℓ_i^{-2} in the unit of square of the mean free path ℓ_e^{-2} and (b) the weighting factors as functions of spin polarization η , where $t_{0,\pm}$ and s represent the WL and WAL channels, respectively. The weighting factors for t_+ and t_- channels are equal.

($\eta = -1$) and $\phi_b = 0$ (2π), the channel t_+ (t_-) gives a pure WL correction as the conventional electron gas.

Temperature dependence of conductivity correction. The integration over q in Eq. (2) is logarithmically divergent in both the ultraviolet and ultra-infrared limit. To avoid the divergence, the two cut-offs have to be introduced to restrict $\ell_\phi^{-1} \leq q \leq \ell_e^{-1}$, where $\ell_e = \sqrt{\mathcal{D}_0\tau}$ is the mean free path and ℓ_ϕ is the coherence length caused by the inelastic scattering [23, 24, 27]. Consequently, Eq. (2) gives the quantum correction to the conductivity,

$$\sigma_{qi}(B=0, T) = \frac{e^2}{\pi h} \sum_i w_i \ln \frac{\ell_\phi^{-2} + \ell_i^{-2}}{\ell_e^{-2} + \ell_i^{-2}}. \quad (3)$$

To investigate the temperature dependence of $\sigma_{qi}(T)$, we assume $\ell_\phi = \ell_\phi^0 (T/T_0)^{-p/2}$, where $p = 1$ for electron-electron interaction and $p = 3$ for electron-phonon interaction in 2D systems, ℓ_ϕ^0 is the coherence length at $T = T_0$ [23, 24]. The characteristic parameter of the temperature-dependent conductivity is [25]

$$\kappa_{qi}^{(n)} \equiv \frac{\pi h}{e^2} \frac{\partial \sigma_{qi}(B=0, T)}{\partial \ln T} = \sum_i \frac{w_i p}{1 + \ell_\phi^2/\ell_i^2} \quad (4)$$

if η and ℓ_e are insensitive to the temperature. In this case, the presence of non-zero Cooperon gap ℓ_i^{-2} is highly non-trivial. As shown in Fig. 4(a), when $\eta = 0$, the conductivity correction is always logarithmically divergent and $\kappa_{qi}^{(n)} = -p/2$. However, once $0 < \eta \ll 1$, $\ell_i^{-2} \neq 0$, the conductivity correction saturates at lower temperatures and $\kappa_{qi}^{(n)}$ would increase from some value $\in (-p/2, 0)$ to 0 gradually. In another limit of $\eta \sim 1$, as shown in Fig. 4(b), $\kappa_{qi}^{(n)} = p/2$ for $\eta = 1$, and $\kappa_{qi}^{(n)}$ decreases from some value $\in (0, p/2)$ to 0 by lowering temperature. Hence, the finite Cooperon gap leads to the saturation behavior of $\sigma_{qi}(0)$ at low temperatures.

In the magnetic TIs, the mass term is related to the magnetization, hence η is also a function of temperature.

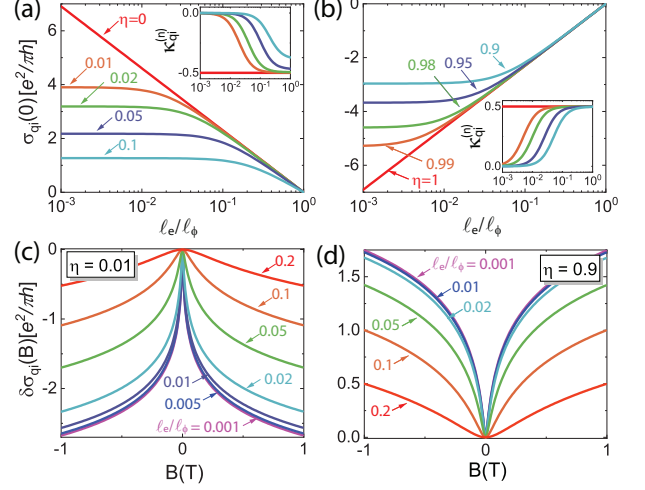


Figure 4. Zero-field conductivity correction and slope $\kappa_{qi}^{(n)}$ as a function of the ratio of the mean free path to the coherence length ℓ_e/ℓ_ϕ for (a) WAL of spin polarization $\eta \sim 0$ and (b) WL of $\eta \sim 1$. Magnetoconductivity at different values of ℓ_e/ℓ_ϕ for (c) $\eta = 0.01$ and (d) $\eta = 0.9$. The calculation parameter $\ell_e = 10\text{nm}$.

Consequently, the slope κ_{qi} has a correction term from $\partial\eta/\partial \ln T$,

$$\kappa_{qi}^{(m)} = \sum_i \left(g_i \frac{\partial \eta}{\partial \ln T} + \frac{w_i p}{1 + \ell_\phi^2/\ell_i^2} \right) \quad (5)$$

with $g_i \equiv \frac{\partial}{\partial \eta} (w_i \ln \frac{\ell_\phi^{-2} + \ell_i^{-2}}{\ell_e^{-2} + \ell_i^{-2}})$. Here we still assume that ℓ_e is insensitive to the temperature. We can have a qualitative analysis for the sign of κ_{qi} for the case of $\eta \sim 0$. When $\eta \sim 0$, $\kappa_{qi}^{(m)} \approx -\frac{\ell_e^{-2} \partial \eta^2 / \partial \ln T + \ell_\phi^{-2} p}{2(\ell_\phi^{-2} + \ell_{i=s}^{-2})}$. If $\frac{\partial \eta}{\partial \ln T} \geq 0$ and $\kappa_{qi} \leq 0$, the zero-field conductivity always decreases with increasing temperature, indicating a WAL tendency as usual. However, if $\frac{\partial \eta}{\partial \ln T} < 0$, $\ell_e^{-2} \frac{\partial \eta^2}{\partial \ln T} < 0$ and $\ell_\phi^{-2} p > 0$, κ_{qi} may experience a sign change while decreasing temperature, which implies anomalous temperature dependence even in the case of the WAL correction. A similar analysis holds for $\eta \sim 1$.

Magnetoconductivity. Experimentally, the effect of quantum interference can be detected by measuring the variation of the conductivity in an external magnetic field. When the magnetic field is along the z -direction, q_x and q_y are quantized into a series of Landau levels as $q_x^2 + q_y^2 \rightarrow (n + \frac{1}{2})\ell_B^{-2}$ with $\ell_B = \sqrt{\frac{\hbar}{4eB}}$ the magnetic length and n a non-negative integer. Consequently, the magnetoconductivity reads [43]

$$\delta\sigma_{qi}(B) = \sum_{i=s, t_\pm} w_i \mathcal{F} \left(\frac{\ell_B^2}{\ell_\phi^2} + \frac{\ell_B^2}{\ell_i^2} \right) \quad (6)$$

where $\mathcal{F}(x) \equiv \frac{e^2}{\pi h} [\psi(x + \frac{1}{2}) - \ln x]$ with $\psi(x)$ the digamma function. Comparing with the previous theories, only

one Cooperon channel was taken into account in the Hikami-Lukin-Nagaoka formula [38] which is valid only in two limits ($\eta = 0$ and $\eta = 1$). In Lu-Shen formula, the two Cooperon channels of triple pairing $i = t_{\pm}$ were approximately treated as one for WL, which forms a competition against the Cooperon channel of singlet pairing ($i = s$) for WAL [25].

When $\eta \ll 1$, Eq. (6) is simplified as $\delta\sigma_{\text{qi}}(B) \approx -\frac{1}{2}\mathcal{F}(\frac{\ell_B^2}{\ell_{\phi s}^2})$ with an effective coherence length $\ell_{\phi s}$: $\frac{1}{\ell_{\phi s}^2} \simeq \frac{\eta^2}{\ell_e^2} + \frac{1}{\ell_{\phi}^2}$. The presence of $\frac{\eta^2}{\ell_e^2}$ means a new decoherence mechanism for the coherence length besides the interaction effect. It is closely related to the correction to the π Berry phase, and becomes dominant at lower temperature as $\frac{1}{\ell_{\phi}^2} \rightarrow 0$. When η is independent of the temperature, as shown in Fig. 4(c), the $\delta\sigma_{\text{qi}}(B)$ gradually saturates when $\ell_e/\ell_{\phi} \rightarrow 0$ as the effective coherence length is approximately determined by $\ell_{\phi s} = \ell_e/\eta$ instead of ℓ_{ϕ} at low temperature. Hence, even a small η can generate an observable effect. When $0 < 1 - \eta \ll 1$, Eq. (6) is simplified as $\delta\sigma_{\text{qi}}(B) \approx \frac{1}{2}\mathcal{F}(\frac{\ell_B^2}{\ell_{\phi t+}^2})$ with $\frac{1}{\ell_{\phi t+}^2} = \frac{(1-\eta)^2}{4\ell_e^2} + \frac{1}{\ell_{\phi}^2}$, where the new decoherence term $\frac{(1-\eta)^2}{4\ell_e^2}$ leads to the saturation of $\delta\sigma_{\text{qi}}(B)$ when $\ell_e/\ell_{\phi} \rightarrow 0$ [See Fig. 4(d)].

This decoherence mechanism corresponds to the decaying Berry phase of multiple scattering trajectories. The Berry phase contributes to the return probability as a phase factor $e^{i\theta} = e^{i\phi_b(1+2n)}$ after n times of revolutions [44]. For $\eta \ll 1$, after averaging over n , we have $\langle e^{i\theta} \rangle \sim -e^{-\eta^2 t/\tau}$, where the minus sign stems from the π Berry phase ($e^{i\pi(1+2n)} = -1$) and gives a WAL correction when $\phi_b \sim \pi$. The decaying factor can reproduce the effective coherence length $\ell_{\phi s}$ in the magnetoconductivity formula for WAL [43]. Furthermore, in the magnetic TIs, η can be a function of the temperature. $\ell_{\phi s}$ or $\ell_{\phi t+}$ can be a non-monotonic function of temperature and further leads to a non-monotonic temperature dependence of magnetoconductivity. In addition, $\delta\sigma_{\text{qi}}(B)$ is still a monotonic function of the magnetic field. Thus, a temperature-dependent η can produce different temperature and magnetic field dependence of magnetoconductivity.

Fitting the experiment. Armed with the formula of magnetoconductivity in Eq. (6), we are now ready to address the puzzle of the anomalous temperature dependence of the conductivity. In Fig. 1, the experimental data labeled by open squares are extracted from the temperature-dependent conductivity at finite B -field in Fig. 4(a)-(c) in Ref. [26]. Since the conductivity correction from the interaction effect is insensitive to the external magnetic field, the magnetoconductivity $\delta\sigma(B)$ can exclude the correction from the interaction effect and is mainly determined by the quantum interference effect, $\delta\sigma(B) \approx \delta\sigma_{\text{qi}}(B)$. For the pristine Bi_2Se_3 of $x_{\text{Mn}} = 0\%$, the Fermi level insects with both the surface band and bulk bands as clearly shown in the ARPES

data in Ref. [26], the $\delta\sigma$ data at different magnetic field can be well fitted by considering one gapless surface states and two gapped bulk sub-bands (solid red lines in Fig. 1a) [36, 41, 48], and the fitting details can be found in Ref. [43].

The magnetoconductivities of the samples of $x_{\text{Mn}} = 4\%$ and $x_{\text{Mn}} = 8\%$ are similar, and turn to increase with decreasing temperature at low temperatures. The anomalous Hall resistivity in a ferromagnetic conductor has an empirical relation with the magnetic field B and magnetization M , $\rho_{xy} = R_0 B + R_{AM}$ [49]. The magnetization is a function of temperature below the Curie temperature T_C . Nonzero magnetization makes the surface states open a tiny gap. For the sample of $x_{\text{Mn}} = 8\%$, from the data of the anomalous Hall resistivity, it is found that M is proportional to $1 - \sqrt{\frac{T}{T_C}}$ below the Curie temperature $T_C = 11.45$ K [50]. η is assumed to obey the same behavior: $\eta(T) = \eta_0[1 - \sqrt{\frac{T}{T_C}}]\Theta(T_C - T)$ (see Sec. SIII.B in Ref. [43]), where η_0 is the spin polarization at the zero temperature, and $\Theta(x)$ is the Heaviside step function. Besides, the mean free path is estimated as $\ell_e \approx 14$ nm at $T = 2$ K and $\ell_e \approx 13.6$ nm at $T = 40$ K from the mobility and carrier density data. ℓ_e is insensitive to temperature and is fixed as 14 nm to reduce the number of fitting parameters. We further assume $\ell_{\phi} = \ell_{\phi}^0 T^{-\delta/2}$ where ℓ_{ϕ}^0 and δ are the fitting parameters and T in unit of Kelvin. In Fig. 1(c), the fitting curves show a good agreement with the experimental data for $B = 0.1, 0.2, 0.5$ and 1 T. The corresponding fitting parameters are listed in the Table SII in Ref. [43]. As the fitting parameter $\eta \simeq 0.2$, the weighting factors $w_{i=t_{\pm}} \simeq 4\eta^2$ and $w_{i=s} \simeq -\frac{1}{2}(1 - 8\eta^2)$. Thus the Cooperon channel of $i = s$ is dominant. Its effective phase coherence length $\ell_{\phi, i=s}$ has a non-monotonic temperature dependence, which is similar to the one given by Tkac et al. [26]. A similar analysis has been applied to the sample of $x_{\text{Mn}} = 4\%$ in Ref. [43], and the fitting curves show a good agreement with the experimental data for $B = 0.2, 0.5, 1$ and 2 T, as displayed in Fig. 1(b). The good coincidence between the theory and the experiment implies that the anomalous temperature dependence of $\delta\sigma$ in the magnetic TIs can be ascribed to the temperature-dependent η or the Berry phase.

Furthermore, we also applied the formula in Eq. (6) to fit the temperature-dependent magnetoconductivity in Cr-doped Bi_2Se_3 ultrathin films in an early measurement [31] by considering two topological surface states and two gapped bulk sub-bands. It was found that the measured crossover from WL to WAL by increasing temperature can be well understood by taking into account the temperature dependence of magnetization of the topological surface states and quantum interference effect of multiple Cooperon channels. Fig. 5(a) shows an excellent agreement between the experimental data and fitting curves, and the corresponding fitting parameters are also consistent at different temperatures. The extracted phase

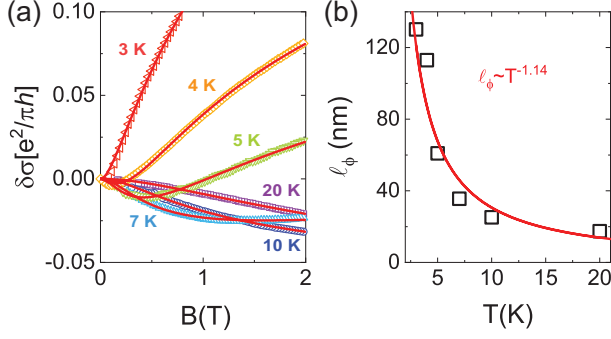


Figure 5. (a) Magnetoconductivity at different temperatures for the Cr-doped Bi_2Se_3 thin film of $x = 0.23$. The open squares are the experimental data extracted from Fig. 2(j) of Ref. [31]. The solid red lines are the fitting results. (b) The temperature dependence of the fitted phase coherence length ℓ_ϕ (open squares). The red line indicates $\ell_\phi \propto T^{-1.14}$.

coherence length follows the power law $\ell_\phi \propto T^{-1.14}$ [see Fig. 5(b)]. More details are referred to Sec. SIV in Ref. [43].

We would like to thank J. Honolka and K. Vyborny for providing original experimental data in Fig. 1. This work was supported by the Research Grants Council, University Grants Committee, Hong Kong under Grant No. 17301717 and C7036-17W.

-
- [1] M. Z. Hasan and C. L. Kane, Rev. Mod. Phys. **82**, 3045 (2010). (document)
 - [2] X. L. Qi and S. C. Zhang, Rev. Mod. Phys. **83**, 1057 (2011).
 - [3] J. E. Moore, Nature **464**, 194 (2010).
 - [4] Y. Ando, J. Phys. Soc. Jpn. **82**, 102001 (2013).
 - [5] S. Q. Shen, *Topological insulators*, 2nd ed. (Springer Nature, Singapore, 2017) (document)
 - [6] D. Culcer, A. Cem Keser, Y. Li, and G. Tkachov, 2D Mater. **7**, 022007 (2020). (document)
 - [7] T. Ando, T. Nakanishi, and R. Saito, J. Phys. Soc. Jpn. **67**, 2857 (1998). (document)
 - [8] H. Suzuura and T. Ando, Phys. Rev. Lett. **89**, 266603 (2002).
 - [9] H. Z. Lu, J. Shi, and S. Q. Shen, Phys. Rev. Lett. **107**, 076801 (2011).
 - [10] H. Z. Lu and S. Q. Shen, Proc. SPIE **9167**, 91672E (2014). (document)
 - [11] J. G. Checkelsky, Y. S. Hor, M. H. Liu, D. X. Qu, R. J. Cava, and N. P. Ong, Phys. Rev. Lett. **103**, 246601 (2009). (document)
 - [12] J. Chen, H. Qin, F. Yang, J. Liu, T. Guan, F. Qu, G. Zhang, J. Shi, X. Xie, C. Yang, *et al.*, Phys. Rev. Lett. **105**, 176602 (2010).
 - [13] H. T. He, G. Wang, T. Zhang, I. K. Sou, G. K. L. Wong, J. N. Wang, H. Z. Lu, S. Q. Shen, and F. C. Zhang, Phys. Rev. Lett. **106**, 166805 (2011).
 - [14] H. Steinberg, J. B. Laloe, V. Fatemi, J. S. Moodera, and P. Jarillo-Herrero, Phys. Rev. B **84**, 233101 (2011).
 - [15] J. Chen, X. Y. He, K. H. Wu, Z. Q. Ji, L. Lu, J. R. Shi, J. H. Smet, and Y. Q. Li, Phys. Rev. B **83**, 241304 (2011).
 - [16] Y. S. Kim, M. Brahlek, N. Bansal, E. Edrey, G. A. Kapilevich, K. Iida, M. Tanimura, Y. Horibe, S.-W. Cheong, and S. Oh, Phys. Rev. B **84**, 073109 (2011). (document)
 - [17] M. Liu, C. Z. Chang, Z. Zhang, Y. Zhang, W. Ruan, K. He, L. I. Wang, X. Chen, J. F. Jia, S. C. Zhang, Q. K. Xue, X. Ma, and Y. Wang, Phys. Rev. B **83**, 165440 (2011). (document)
 - [18] J. Wang, A. M. DaSilva, C. Z. Chang, K. He, J. K. Jain, N. Samarth, X. C. Ma, Q. K. Xue, and M. H. W. Chan, Phys. Rev. B **83**, 245438 (2011).
 - [19] Y. Takagaki, B. Jenichen, U. Jahn, M. Ramsteiner, and K. J. Friedland, Phys. Rev. B **85**, 115314 (2012).
 - [20] H. C. Liu, H. Z. Lu, H. T. He, B. Li, S. G. Liu, Q. L. He, G. Wang, I. K. Sou, S. Q. Shen, and J. Wang, ACS nano **8**, 9616 (2014).
 - [21] W. J. Wang, K. H. Gao, and Z. Q. Li, Sci. Rep. **6**, 25291 (2016). (document)
 - [22] Y. Jing, S. Huang, K. Zhang, J. Wu, Y. Guo, H. Peng, Z. Liu, and H. Xu, Nanoscale **8**, 1879 (2016). (document)
 - [23] B. L. Altshuler, A. G. Aronov, and P. A. Lee, Phys. Rev. Lett. **44**, 1288 (1980). (document)
 - [24] P. A. Lee and T. V. Ramakrishnan, Rev. Mod. Phys. **57**, 287 (1985). (document)
 - [25] H. Z. Lu and S. Q. Shen, Phys. Rev. Lett. **112**, 146601 (2014). (document)
 - [26] V. Tkac, K. Vyborny, V. Komanicky, J. Warmuth, M. Michiardi, A. Nganku, M. Vondracek, R. Tarasenko, M. Valiska, V. Stetsovych, *et al.*, Phys. Rev. Lett. **123**, 036406 (2019). (document), 1
 - [27] A. L. Efros and M. Pollak, *Electron-electron interactions in disordered systems* (Elsevier, Amsterdam, 1985). (document)
 - [28] Q. Liu, C. X. Liu, C. Xu, X. L. Qi, and S. C. Zhang, Phys. Rev. Lett. **102**, 156603 (2009). (document)
 - [29] Y. S. Hor, P. Roushan, H. Beidenkopf, J. Seo, D. Qu, J. G. Checkelsky, L. A. Wray, D. Hsieh, Y. Xia, S.-Y. Xu, D. Qian, M. Z. Hasan, N. P. Ong, A. Yazdani, and R. J. Cava, Phys. Rev. B **81**, 195203 (2010).
 - [30] Y. Chen, J. H. Chu, J. Analytis, Z. Liu, K. Igarashi, H. H. Kuo, X. Qi, S.-K. Mo, R. Moore, D. Lu, *et al.*, Science **329**, 659 (2010).
 - [31] M. Liu, J. Zhang, C. Z. Chang, Z. Zhang, X. Feng, K. Li, K. He, L. I. Wang, X. Chen, X. Dai, Z. Fang, Q. K. Xue, X. Ma, and Y. Wang, Phys. Rev. Lett. **108**, 036805 (2012). (document), 5
 - [32] Y. Tokura, K. Yasuda, and A. Tsukazaki,

- Nat. Rev. Phys. **1**, 126 (2019). (document)
- [33] W. Y. Shan, H.-Z. Lu, and S. Q. Shen, New J. Phys. **12**, 043048 (2010). (document)
- [34] H. Z. Lu, W. Y. Shan, W. Yao, Q. Niu, and S. Q. Shen, Phys. Rev. B **81**, 115407 (2010). (document)
- [35] Y. Zhang, K. He, C. Z. Chang, C. L. Song, L. L. Wang, X. Chen, J. F. Jia, Z. Fang, X. Dai, W. Y. Shan, *et al.*, Nat. Phys. **6**, 584 (2010). (document)
- [36] H. Z. Lu and S. Q. Shen, Phys. Rev. B **84**, 125138 (2011). (document)
- [37] L. Gorkov, A. Larkin, and D. KhmelNitskii, JETP Lett. **30**, 248 (1979). (document)
- [38] S. Hikami, A. I. Larkin, and Y. Nagaoka, Prog. Theor. Phys. **63**, 707 (1980). (document)
- [39] G. Bergmann, Phys. Rep. **107**, 1 (1984).
- [40] E. McCann, K. Kechedzhi, V. I. Falko, H. Suzuura, T. Ando, and B. L. Altshuler, Phys. Rev. Lett. **97**, 146805 (2006).
- [41] I. Garate and L. Glazman, Phys. Rev. B **86**, 035422 (2012). (document)
- [42] B. Fu, H. W. Wang, and S. Q. Shen, Phys. Rev. Lett. **122**, 246601 (2019). (document)
- [43] See Supplemental Material at [URL to be added by publisher] for details of SI. The microscopic theory of quantum interference, SII. The calculation of the Cooperon structure factor and Hikami box, SIII. The experimental fitting for the samples of $x_{Mn} = 0\%$, $x_{Mn} = 4\%$, and $x_{Mn} = 8\%$, and SIV. The experimental fitting for the sample of Cr doped TI thin film, which includes Refs.[21, 22, 26, 31, 35, 38, 42, 44–47]. (document)
- [44] I. Gornyi, V. Y. Kachorovskii, and P. Ostrovsky, Phys. Rev. B **90**, 085401 (2014). (document)
- [45] J. J. Lin, and J.P. Bird, J. Phys. Condens. Matter., **14**, R501-R596 (2002).
- [46] Z. Li, T. Chen, H. Pan, F. Song, B. Wang, *et al.*, Sci. Rep., **2**, 595(2012).
- [47] E. Akkermans, and G. Montambaux. *Mesoscopic physics of electrons and photons* (Cambridge university press, England, 2007). (document)
- [48] H. Velkov, G. N. Bremm, T. Micklitz, and G. Schwiete, Phys. Rev. B **98**, 165408 (2018). (document)
- [49] N. Nagaosa, J. Sinova, S. Onoda, A. H. MacDonald, and N. P. Ong, Rev. Mod. Phys. **82**, 1539 (2010). (document)
- [50] The Curie temperature T_C deduced from the anomalous Hall resistivity here is different from the one obtained by Tkac *et al.* [26]. A possible explanation for this discrepancy could lie in the different techniques or in the inhomogeneity of the sample, which is not unexpected for such dilute magnetic systems. (document)